Journal of Magnetic Resonance 248 (2014) 115–125

Contents lists available at ScienceDirect

Journal of Magnetic Resonance

journal homepage: www.elsevier.com/locate/jmr

A double-component Anderson–Weiss approach for describing NMR signals of mobile SI_n units: Application to constant-time DIPSHIFT experiments

Marcio Fernando Cobo [a,*], Detlef Reichert [b], Kay Saalwächter [b,*], Eduardo Ribeiro deAzevedo [a,*]

[a] Instituto de Física de São Carlos, Universidade de São Paulo, Caixa Postal 369, CEP, 13560-970 São Carlos, São Paulo, Brazil
[b] Institut für Physik – NMR, Martin-Luther-Universität Halle-Wittenberg, Betty-Heimann-Str. 7, D-06120 Halle, Germany

ARTICLE INFO

Article history:
Received 8 May 2014
Revised 11 September 2014
Available online 28 September 2014

Keywords:
Nuclear magnetic resonance spectroscopy
Magic-angle spinning
Organic solids
Heteronuclear dipole–dipole couplings
Dynamics
Anderson–Weiss approximation
DIPSHIFT

ABSTRACT

A composed Gaussian local field is proposed to describe the effect of molecular motions on NMR signals of SI_n units (e.g., CH_n or NH_n), based upon the well-know Anderson–Weiss (AW) approximation. The approach is exemplified on constant-time recoupled dipolar chemical-shift correlation (t_C-recDIPSHIFT) experiments, providing an analytical formula that can be used as a fitting function in studies of intermediate-regime motions. By comparison of analytical t_C-recDIPSHIFT curves and dynamic spin dynamics simulations, we show that for heteronuclear spin pairs (SI system), the AW treatment assuming the usual Gaussian local field is accurate. However, the approximation fails for the case of SI_n spin systems for motional rates higher than a few kHz. Based on earlier work of Terao et al., who proposed a decomposition of CH_n dipolar powder patterns into to 2^n spin-pair-type patterns, we propose an AW approach based upon a double-Gaussian local field. We derive an analytical formula for t_C-recDIPSHIFT signals, and demonstrate its accuracy by comparison with simulations of several motional geometries and rates, and with experimental results for a model sample. The approach is not limited to the t_C-recDIPSHIFT experiment and should be of general use in dipolar-coupling based experiments probing (partially) mobile SI_n molecular moieties.

1. Introduction

Molecular dynamics exerts a fundamental role in the function of many soft and solid organic materials [1–6]. Its well known that properties of construction polymers, such as brightness and resistance to shear, creep and tension, are all intimately related to the local segmental dynamics of the polymer chains. This is also true for more advanced materials, such as nano-structured copolymers or hybrids, where the clever combination of components with distinct dynamic properties lead to composite systems with tunable mechanical behavior. However, not only the mechanical properties are sensitively affected by molecular dynamics. For example, in semiconducting polymers the charge transport and light emission properties are sensitive to changes in the polymer chain dynamics, and in host–guest systems for sensor applications the conformational switching is intrinsically associated with rearrangement of the guest molecules. Last but not least, in biological solids the importance of molecular dynamics is even more recognized, being intimately related to the system function [7].

Thus, the understating of internal and segmental dynamics becomes crucial for establishing a bridge between molecular properties and function. In this sense, the toolbox of solid-state NMR provides many methods capable of elucidating details of local and segmental dynamics in solid and "soft", possibly biomolecular organic materials [8–13], and many exemplary studies have been reported [2,3,5,14,4,15–19].

An important feature for a technique be used in studies of molecular dynamics is the ability to characterize the timescale (the correlation time or its inverse, the motional rate) of the motion over a wide dynamic range. This usually involves the application of several dynamic NMR methods, covering different time windows [8,20]. Among them are the separated local-field (SLF) methods focussing on the motion of heteronuclear SI_n dipolar tensors, which have been first developed for structural studies [21–23], and later became a recognized and important tool for determining order parameters of fast-limit molecular motions [24–26].

* Corresponding authors.
E-mail addresses: marciofcobo@gmail.com (M.F. Cobo), kay.saalwaechter@physik.uni-halle.de (K. Saalwächter), azevedo@ifsc.usp.br (E.R. deAzevedo).

http://dx.doi.org/10.1016/j.jmr.2014.09.009
1090-7807/

More recently, we have shown that SLF experiments, specifically the dipolar chemical-shift correlation (DIPSHIFT) and Lee–Goldburg cross-polarization (LGCP) experiments, can also be used to extract the rate of molecular motions in the intermediate regime, i.e., rates in the μs to ms range [27,28]. This was achieved by comparison of experimental results and theoretical calculations by using either numerical simulations [29,30] or analytical fitting formulas based on the Anderson–Weiss (AW) approximation [31,32].

The next step was the augmentation of the dynamic window and the sensitivity to small-angle motions in DIPSHIFT experiments by introducing REDOR-type recoupling, which was dubbed as T_2-recDIPSHIFT [33]. In this method, molecular motions are reflected in both the apparent averaging of the dipolar coupling and a T_2-type intensity decay when the dynamics is in the intermediate regime. However, due to signal-function symmetry reasons, it was so far not possible to develop a fully analytical approximation to describe the T_2-recDIPSHIFT experiments. We here present the derivation and a thorough test of an AW-based fitting formula for an earlier variant [34] of the recoupled DIPSHIFT experiment based upon constant-time recoupling (t_C-recDIPSHIFT), recognizing that this experiment does not have the mentioned limitation. It is based upon a simple incremented time shift of the REDOR π pulse positions, holding all other pulse sequence timings constant. While this experiment has a narrower dynamic window than T_2-recDIPSHIFT because the data does not show an apparent T_2 effect, t_C-recDIPSHIFT is more robust and less prone to setup problems and other experimental imperfections [33].

Based on the AW approach [31] recently extended by Hirschinger [32], the analytical formula now allows to use t_C-recDIPSHIFT to study intermediate-regime motions in solids via a simple fitting procedure to the experimental data, which is a great advantage and enhances the practical applicability of the technique. The resulting molecular-dynamic parameters are the order parameter and the motional rate, both being reflected in the apparent averaging of the dipolar interaction tensor between chemically bonded nuclei. In order to ascertain the accuracy and the limits of validity of the approach, we compare the analytical t_C-recDIPSHIFT curves with results of dynamic spin dynamics simulations [30] for different spin systems and geometries of motion. We also demonstrate that the usual AW approximation fails in the description of t_C-recDIPSHIFT signals of CH_n multiplets. We thus suggest an AW approach based upon a double-Gaussian local field and demonstrate its reliability in describing t_C-recDIPSHIFT results. However, once it is possible to obtain a resolved ^{13}C MAS spectrum and to probe the evolution of the resonances under specific CH coupling, there is no serious limitation for the use of the presented AW approximation in describing the motion effects on the signals obtained by other techniques. Therefore, since the use of this strategy is not limited to the t_C-recDIPSHIFT experiment but can easily be generalized, we consider the double-Gaussian AW approach to describe the signal of mobile CH_n multiplets a step forward and expect a wide range of applications.

2. Experimental

The t_C-recDIPSHIFT pulse sequence, bracketed between two z-filters and preceded by CP-based excitation of ^{13}C, is shown in Fig. 1a. The experiments were performed on a Varian Inova 400 spectrometer, using a Jakobsen 7 mm WVT double-resonance probe. A MAS frequency of 6 kHz, a ^{13}C pulse width of 3.5 μs and an (effective) RF power for the Lee–Goldburg (LG) homonuclear and heteronuclear decoupling of 62.3 kHz (CW during DIPSHIFT evolution and TPPM during acquisition) were used. Trimethylsulfoxonium iodide (TMSI), see the formula in Fig. 1b, was used as a model sample to experimentally verify the accuracy of the proposed double-Gaussian AW-based approach for calculating t_C-recDIPSHIFT modulation curves. We also compare the theory with full dynamic spin dynamics simulations using the SPINEVOLUTION simulation program [30]. The program was custom-modified by M. Veshtort to implement arbitrary rotational jump motions.

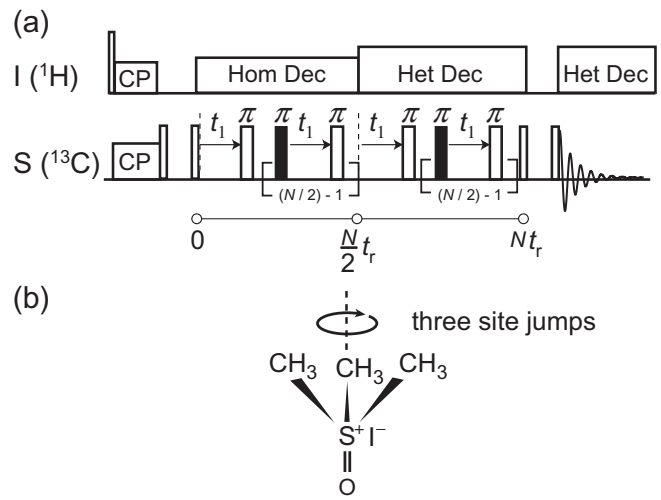

Fig. 1. (a) Scheme of the t_C-recDIPSHIFT pulse sequence, which amplifies the effects of the IS dipole–dipole interaction by N as compared with original DIPSHIFT experiment. (b) Sketch of the trimethylsulfoxonium iodide (TMSI) molecule, which performs a molecular jump motion around its C_3 symmetry axis. The ^1H nuclei further undergo fast rotations about the internal C_3 axis of the CH_3 groups.

3. Theory

3.1. Accessing molecular dynamics using t_C-recDIPSHIFT

t_C-recDIPSHIFT [34] is an SLF NMR experiment that is designed to accurately measure heteronuclear dipole–dipole couplings between abundant (I, often ^1H) and rare (S, often ^{13}C or ^{15}N) nuclear spins in order to probe molecular conformation [34] or motions [33]. The pulse sequence is based upon the original DIPSHIFT experiment [21], but with the effect of the heteronuclear dipole–dipole couplings amplified by a factor N, which is achieved by a REDOR-type π pulse train [35]. This amplification renders the technique particularly suitable for applications in weakly coupled spin systems, or to probe small-amplitude molecular motions.

As the experiment is based upon a common CP MAS experiment, it allows for an assessment of the S–I_n dipole–dipole coupling tensors for each resolved chemical site of S; for S = ^{13}C and not too large molecules, it easily applicable in natural abundance. Further, the actual t_C-recDIPSHIFT part between the two z-filters (see Fig. 1a) can be easily implemented in higher-dimensional spectra. After the first z-filter, the S transverse magnetization evolves during $N/2$ rotor periods ($(N/2)t_r$) under homonuclear decoupling (simple Lee–Goldburg irradiation or its variants [36,37]) of the I nuclei, allowing for S-spin evolution under the S–I_n heteronuclear dipole–dipole coupling. During the second half, heteronuclear decoupling is applied. Chemical-shift refocusing is ensured by the omission of the central π pulse of the REDOR recoupling π pulse train applied to S, for which the pulses are nominally spaced by $t_r/2$.

To achieve a coupling-sensitive intensity modulation, the temporal position of every other π pulse (open bars in Fig. 1a) is varied according to the parameter t_1, ranging from 0 to t_r. This constitutes a constant-time period of $(N/2)t_r$, during which the detected intensity is modulated by the evolution under the S–I_n coupling, being

amplified by a factor of N as compared to the original DIPSHIFT experiment. As molecular motions change the S–I$_n$ coupling, a fit of the modulation curve with suitably simulated or modeled data, it is possible to access dynamic information such as a dipolar dynamic order parameter

$$S_{\mathrm{dip}} = \sqrt{\frac{M_2^{\mathrm{HT}}}{M_2^{\mathrm{LT}}}} \tag{1}$$

and also the motional rate. In the above equation, M_2^{HT} and M_2^{LT} are the high-temperature (fast-motion limit) and low-temperature (rigid-limit) second moments of the dipolar local field, respectively. For a powder of isolated SI spin pairs, we simply have

$$M_2^{\mathrm{LT}} = \gamma_I^2\gamma_S^2/(5r_{IS}^6) = (1/5)(D_{\mathrm{rig}})^2, \tag{2}$$

with D_{rig} being the dipole–dipole coupling constant in rad/s [38]. Note that for heteronuclear spins the prefactor 1/5 is different from the commonly known value of 9/20 for homonuclear coupling.

3.2. The Anderson–Weiss approach for t_C-recDIPSHIFT experiments

Anderson–Weiss (AW) theory [31], also known as Gaussian frequency distribution model, is particularly suitable to analytically evaluate effects of molecular motion on NMR signals [39,40,32,27,28,41,42]. Thanks to the Gaussian-distribution assumption for the local field, the signal is completely described by a memory function $K(\tau)$ that takes into account the pulse sequence features and the molecular-motion effects:

$$S(t) = \exp\left\{-\int_0^t (t-\tau)K(\tau)\mathrm{d}\tau\right\}. \tag{3}$$

We note that the real frequency distribution for isolated S–I$_n$ moieties is of course Pake-like, but, as shown in the above-cited papers, approximating it by a Gaussian function does not introduce serious errors for time-domain signals as long as the evolution times are not too large as compared to the inverse effective coupling.

For the t_C-recDIPSHIFT pulse sequence, the memory function is written in terms of [39,40,32] (i) the modulation in the heteronuclear dipole–dipole interaction arising from the MAS, (ii) the effects of the S-spin pulses, here assumed to be delta pulses and (iii) the loss of phase correlation due to molecular motion.

In the present approach, the homonuclear decoupling is not explicitly taken into account, and a simple scaling factor is introduced to account for the tilted effective field during LG irradiation. Further, perfect heteronuclear decoupling and chemical-shift refocusing are assumed, such that the calculations can be limited to the first $(N/2)t_r$ of actual dipolar evolution. An AW-based expression for the S-spin signal under recoupling of the heteronuclear IS interaction has already been derived in Ref. [32]. Using this expression, the fitting function for the S-spin signal $S(t)$, obtained at an arbitrary time t after the application of N_P recoupling pulses becomes

$$S(t > t_{N_p}) = \exp\left\{s \times M_2^{\mathrm{HT}}\left[\frac{2}{3}F_{N_p}(0,\omega_r,t) + \frac{1}{3}F_{N_p}(0,2\omega_r,t)\right] + s \times \left(M_2^{\mathrm{LT}} - M_2^{\mathrm{HT}}\right)\left[\frac{2}{3}F_{N_p}(k,\omega_r,t) + \frac{1}{3}F_{N_p}(k,2\omega_r,t)\right]\right\}. \tag{4}$$

Here,

$$F_{N_p}(k,n\omega_r,t) = \frac{1}{k^2+(n\omega_r)^2}\left\{(2N_P+1)\frac{k^2-(n\omega_r)^2}{k^2+(n\omega_r)^2} - kt - (-1)^{N_p}h_-^{(n)}(t) + 4\sum_{i=1}^{N_p}\sum_{j>i}^{N_p}(-1)^{j-i}h_+^{(n)}(t_i-t_j) + 2\sum_{j=1}^{N_p}(-1)^j\left[h_-^{(n)}(t_j) - (-1)^{N_p}h_-^{(n)}(t-t_j)\right]\right\}, \tag{5}$$

and

$$h_\pm^{(n)}(t) = \frac{\exp(\pm kt)}{k^2+(n\omega_r)^2}\left[(k^2-(n\omega_r)^2)\cos(n\omega_r t) \pm 2kn\omega_r\sin(n\omega_r t)\right]. \tag{6}$$

t_j is the temporal position of the jth recoupling π pulse, N_p is the total number of applied recoupling pulses, which relates with the amplification factor N as $N_p = N-1$. ω_r is the MAS frequency in rad/s and $k = 1/(n_{sites}\tau_c)$ is the rate of motion, where n_{sites} is the number of accessible sites and τ_c is the correlation time of the molecular motion. The scaling factor s accounts for an apparently reduced second moment, for instance due to the application of LG decoupling ($s = f_{\mathrm{LG}}^2$ with $f_{\mathrm{LG}} = 0.577$) or other experimental factors, as will be discussed.

For the particular case of the t_C-recDIPSHIFT experiment, see Fig. 1a, the signal is evaluated at $t = (N/2)t_r$ for several temporal positions of the recoupling pulses, which can be expressed in terms of t_r and t_1 (ranging from 0 to t_r) as

$$t_{2j} = jt_r$$
$$t_{2j+1} = jt_r + t_1$$

Therefore, for the t_C-recDIPSHIFT curves, the signal calculated by Eq. (4) will be explicitly dependent on t_1, $S(t_1)$. For instance, we calculate the signal of the t_C-recDIPSHIFT experiment for $N = 2$ by setting $N_P = 1$ $t = t_r$ with t_1 ranging from 0 to t_r.

4. Results and discussion

4.1. MAS dependence of the Gaussian local field approximation for I–S dipolar coupled spins

Because of spin diffusion, the dipolar powder in strongly coupled multi-spin homonuclear systems, for instance ^{1}H nuclei in organic materials, is very well represented by a Gaussian function (Van Vleck theory [43]), making the AW approximation always valid. In contrast, the dipolar powder of heteronuclear spin systems present specific features which are not reproduced in the Gaussian powder approximation. However, it has been shown that for evolution times shorter than the inverse of the heteronuclear dipolar coupling, the time evolution of a given spin S dipolar coupled to a spin I can be well described by the so called second moment approximation [44]. In rigid systems, this is of course equivalent to the Gaussian approximation for the local field, i.e., AW treatment [27].

Besides, in MAS experiments the rotation frequency also play a role in limiting the validity of the Gaussian approximation. In the context of DIPSHIFT experiments, this was earlier explored in Ref. [27], where we show that the AW based fitting formula could only be used at higher MAS frequency, which was chosen based on the matching between the shape of the rigid limit experimental DIP-

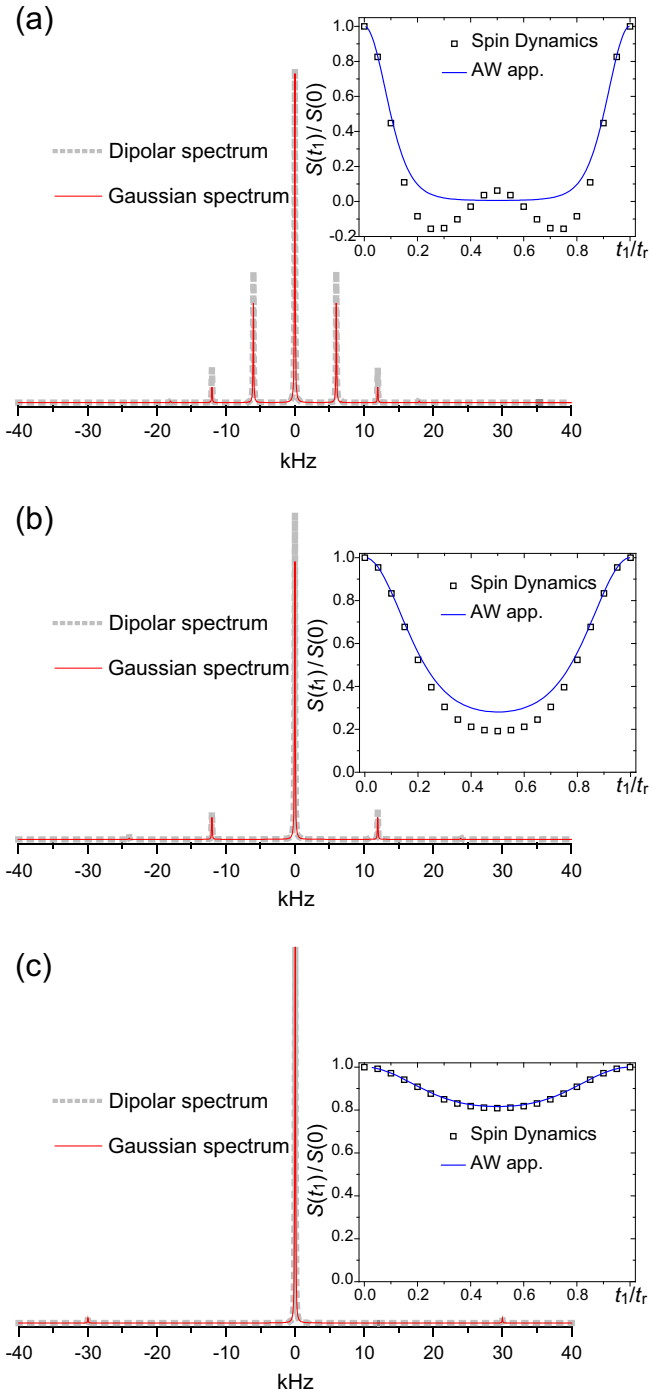

Fig. 2. MAS dipolar spectrum of rigid CH powder under LG irradiation at MAS rates of (a) 6 kHz, (b) 12 kHz and (c) 30 kHz. Dipolar spectrum refers to the calculation using the actual dipolar coupling while Gaussian spectrum refer to the spectrum calculated using a Gaussian local field approximation. In the corresponding insets are simulated $2t_r$-t_C-recDIPSHIFT curves (spin dynamics) and the AW Gaussian approximation using the same second moment ($M_2^{LT} = 40.66 \times 10^8$ (rad/s)^2) multiplied by the scaling factor $(f_{LG})^2 = 0.333$).

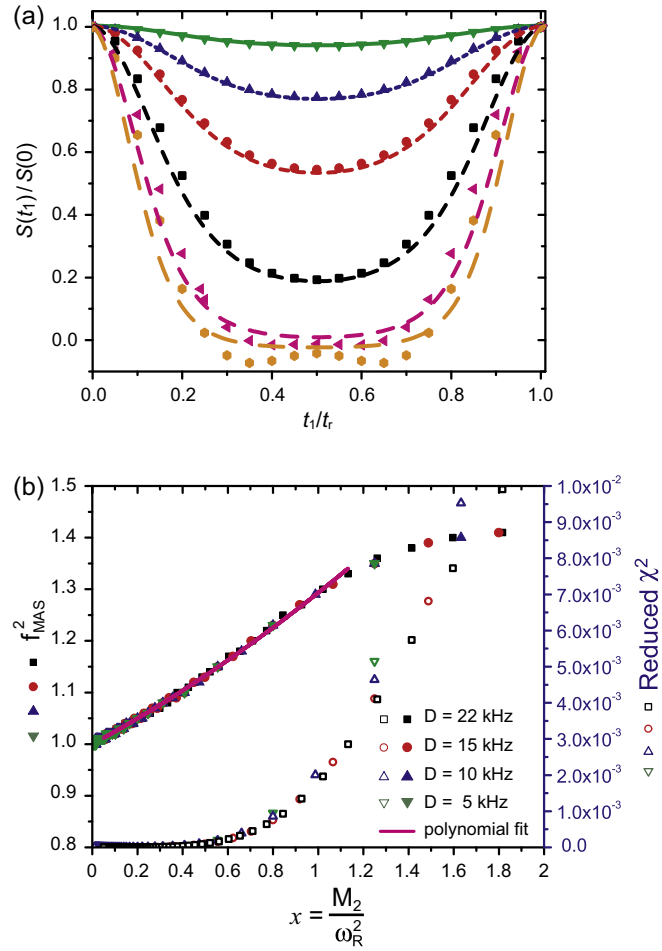

Fig. 3. (a) Comparison between simulated $2t_r$-t_C-recDIPSHIFT and the corresponding curves calculated according to Eq. (4) with M_2 value scaled by a best-fit factor $s = (f_{MAS})^2 \times (f_{LG})^2$ with fixed $f_{LG} = 0.577$. Spin dynamics simulations are show as up triangles: $M_2/\omega_r^2 = 0.035$; down triangles: $M_2/\omega_r^2 = 0.140$; circles: $M_2/\omega_r^2 = 0.313$; squares: $M_2/\omega_r^2 = 0.701$; horizontal triangles: $M_2/\omega_r^2 = 1.250$; diamonds: $M_2/\omega_r^2 = 1.582$. The lines are the corresponding best fit curves using Eq. (4), proving f_{MAS} values of 1.01, 1.03, 1.08, 1.2, 1.36, 1.4. (b) Plot of f_{MAS}^2 as a function of the reduced second moment $x = M_2/\omega_r^2$ obtained by similar fit as in (a) using several M_2 and MAS frequencies. The reduced-χ^2 coefficients obtained from the fitting are also plotted. The polynomial fitting function is $f_{MAS}^2 = 1 + 0.047x + 0.0022x^2$.

SHIFT curve with that calculated using the AW fitting formula. Thus, before analyzing the validity of Eq. (4) for describing motion effects in t_C-recDIPSHIFT experiments, we discuss its accuracy in the rigid limit, mainly concerning the MAS dependence.

The main point to be considered is whether the t_C-recDIPSHIFT curve can be approximated by an AW formula using the same second moment as the actual dipolar pattern. To verify this, we simulated the $2t_r$-t_C-recDIPSHIFT curves for a powder of CH coupled spins with the dipolar coupling (D_{rig}) scaled down by f_{LG} and compare with curves calculated using Eq. (4) evaluated with the same second moment as the corresponding CH powder [38], varying the MAS frequency and D_{rig}. Fig. 2a–c shows the MAS dipolar spectra of a rigid CH spin pair powder as well as the corresponding t_C-recDIPSHIFT curves (inset) obtained using spin dynamics simulations and Eq. (4). At low MAS frequencies (6 kHz) both the sideband pattern and the $2t_r$-t_C-recDIPSHIFT curves calculated using Eq. (4) are considerably different from those obtained using the spin dynamics simulations. At moderate spinning frequencies (12 kHz), despite exhibiting the right shape, Eq. (4) still fails in reproducing the t_C-recDIPSHIFT curve obtained with the actual dipolar pattern. At high MAS frequencies (30 kHz), both the MAS pattern and the $2t_r$-t_C-recDIPSHIFT curve are perfectly reproduced by Eq. (4). This behavior indicates that the use of Eq. (4) for calculating t_C-recDIPSHIFT curves is indeed more accurate in ultra-fast MAS experiments, which is becoming quite popular due to the recent developments in high spinning probe technology [45–47].

Yet, since most of the applications are still done in conventional MAS probes (spinning frequencies up to 20 kHz), it is crucial to ver-

ify the validity of the AW approach for dynamical studies at moderate MAS spinning frequencies. As seen in Fig. 2b, in this moderate spinning frequency regime, the overall shape of the $2t_r$-t_C-recDIPSHIFT curve is well reproduced, so by adding an extra scaling to the second moment $\left(s = (f_{MAS} \times f_{LG})^2\right)$, the $2t_r$-t_C-recDIPSHIFT curve is nicely reproduced, as shown in Fig. 3a. This suggests the possibility of using scaled second moments $s \times M_2$ to calculate the motion sensitive t_C-recDIPSHIFT curves using Eq. (4) at moderate MAS frequencies.

Simulations as those shown in the inset of Fig. 2 were performed for various coupling values and MAS rates and fitted using Eq. (4) to obtain the scaling factor f^2_{MAS} as a function of the second moment and MAS rates. Some of the spin dynamics simulations and the corresponding best fits are shown in Fig. 3a. Fig. 3b shows the best fit f^2_{MAS} values as a function of the reduced second moment M_2/ω_r^2. This plot provides a master curve which is seen to provide a consistent measure of the necessary additional scaling. As it can be seen, f^2_{MAS} gives a correction related to the non-trivial shape of the modulation curve when it is not matched by the AW approximation. Indeed the accuracy of the approximation can be quantified by the Reduced χ^2 value extracted from the fit. As depicted in Fig. 3, by taking a lower threshold of 0.001 for the Reduced χ^2, one can establish that the limit for using the AW approximation in the DIPSHIFT experiments is $M_2/\omega_r^2 < 1$, which gives a good parameter for deciding the minimum MAS rate that the experiments should be run. Indeed, in the limit $M_2/\omega_r^2 < 1$ the f^2_{MAS} vs. M_2/ω_r^2 curve is well reproduced by a second order polynomial. For practical use, the figure caption indicates the polynomial used to fit and this predict this universal dependence. Alternatively, the experimental curve measured at low (rigid limit) and high temperatures (fast limit) can of course be fitted with Eq. (4) in order to directly extract the scaled second moments.

4.2. Comparison of the AW approach and dynamic spin dynamics simulations

As shown in Ref. [27], the AW approximation for evaluating DIPSHIFT NMR signals only holds for evolution periods shorter than the inverse of the dipolar coupling. This is primarily due to the failure of the second-moment approximation for the local field at longer evolution periods, where the particularities of the distribution (higher moments) become important. Besides, the typical T_2 decay in the DIPSHIFT experiment may not be reproduced by an AW-based approximation. In this respect, the t_C-recDIPSHIFT behaves differently, since the sensitivity to the rate of motion arises only from the apparent averaging effect of the dipolar coupling. For a demonstration, in Fig. 4a–c we compare $2t_r$-t_C-recDIPSHIFT curves calculated via full dynamic spin dynamics simulations (symbols) with those obtained using the AW approximation (lines), Eq. (4), considering several motional rates. In the curves calculated using Eq. (4), the scaled second moments $s \times M_2^{HT}$ and $s \times M_2^{LT}$ were obtained by fitting the fast-limit and rigid curves, i.e., they are actually the second moment multiplied by $\left(f^{HT}_{MAS} \times f_{LG}\right)^2$ and $\left(f^{LT}_{MAS} \times f_{LG}\right)^2$, respectively. Note that because of the different dipolar couplings $f^{LT}_{MAS} \neq f^{HT}_{MAS}$. Fig. 4a shows CH spin pair simulations, mimicking a two-site jump with a reorientation angle of 120°, as indicated in the inset. Clearly, the AW approximation holds in this case, being valid for the whole evolution time window of the experiment.

The possibility of reproducing the complete t_C-recDIPSHIFT curve with the proposed AW-based fitting function is an intrinsic advantage over the T_2-dependent DIPSHIFT variants [27,33]. However, increasing the number of ^{1}H attached to the carbon, the AW approach fails to describe the $2t_r$-t_C-recDIPSHIFT data. This is demonstrated in Fig. 4b, which presents a comparison between full spin dynamics simulations and AW-based curves for a CH_2 group executing a planar three-site jump (see the geometry in the inset). The AW approach holds for slower motional rates $k = 3$ kHz, but the agreement becomes worse at higher rates.

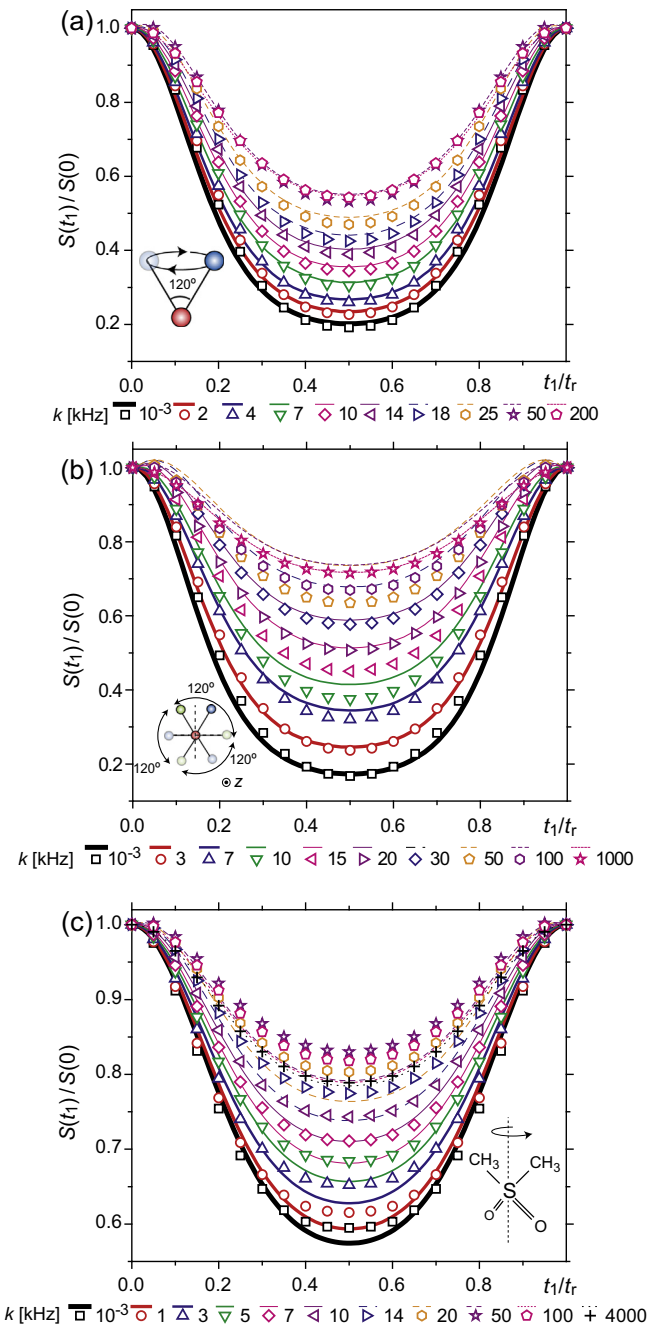

Fig. 4. Comparison between the AW approximation (lines) and dynamic spin dynamics simulations (symbols) for $2t_r$-t_C-recDIPSHIFT curves. (a) CH group performing a two-site jump with reorientation angle of 120°, $\nu_r = 12$ kHz, $s \times M_2^{LT} = 17.08 \times 10^8$ (rad/s)^2 and $s \times M_2^{HT} = 6.50 \times 10^8$ (rad/s)^2. (b) CH_2 group performing a planar three-site jump with amplitude of motion of 120°, $\nu_r = 16$ kHz, $s \times M_2^{LT} = 33.27 \times 10^8$ (rad/s)^2 and $s \times M_2^{HT} = 6.30 \times 10^8$ (rad/s)^2. (c) CH_3 group performing a two-site jump with the DMS geometry, $\nu_r = 9$ kHz, $s \times M_2^{LT} = 33.25 \times 10^7$ (rad/s)^2 and $s \times M_2^{HT} = 14.54 \times 10^7$ (rad/s)^2.

Another example is shown Fig. 4c, which features the same comparison for the case of a CH_3 group executing two-site jumps with reorientation angle of 109°, including an internal fast permutation of the CH_3 protons. This corresponds to the motion executed

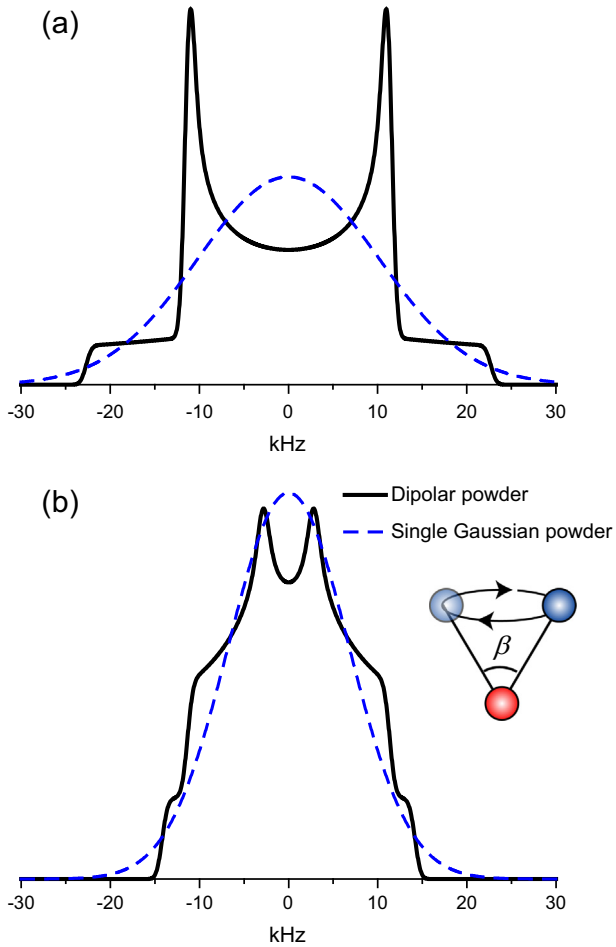

Fig. 5. CH dipolar powder patterns and corresponding Gaussian approximations with the same second moment (a) in the rigid limit with $M_2^{LT} = 40.66 \times 10^8$ (rad/s)^2 and (b) in the fast limit for a two-site jump with $\beta = 120°$ and $M_2^{HT} = 17.80 \times 10^8$ (rad/s)^2. To improve the visualization, the dipolar powder was Gaussian broadened by 500 Hz, but its second moment was calculated from the pattern without any broadening.

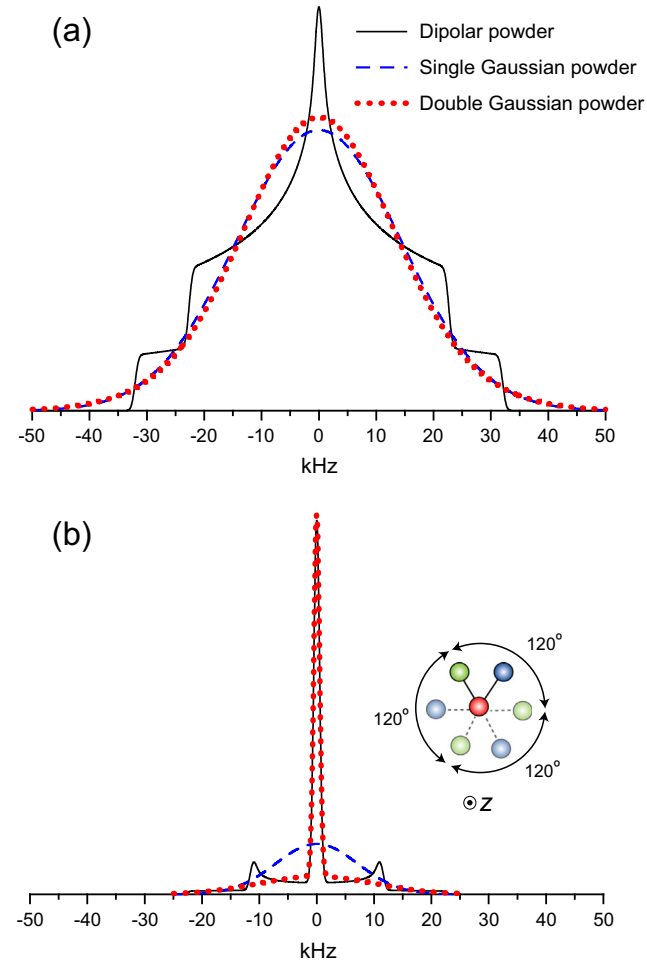

Fig. 6. CH_2 dipolar powder patterns and corresponding Gaussian approximations. (a) In the rigid limit the dipolar powder as well as the single Gaussian approximation have $M_2^{LT} \sim 81.14 \times 10^8$ (rad/s)^2 while the double Gaussian approximation is the sum of two Gaussian lines with $M_2^{LT} \sim 54.07 \times 10^8$ (rad/s)^2 and $M_2^{LT} \sim 108.20 \times 10^8$ (rad/s)^2. (b) In the fast limit the dipolar powder as well as the single Gaussian approximation have $M_2^{HT} \sim 20.32 \times 10^8$ (rad/s)^2 while the double Gaussian approximation is the sum of two Gaussian lines with $M_2^{HT} \sim 40.51 \times 10^8$ (rad/s)^2 and $M_2^{HT} \sim 0$ (rad/s)^2. To improve the visualization, the dipolar powder was Gaussian broadened by 500 Hz, but the presented second moments were calculated from the pattern without any broadening, so the Gaussian shape of the central peak in (b) is only due to line broadening.

by the CH_3 groups in dimethyl sulfone (DMS) molecular crystals, of course assuming the protons permutation belonging to the methyl group to be in the fast limit. Again, the AW approximation is not suitable to describe the curve for rates higher than 3 kHz. Cases of molecular motions with different geometries and numbers of sites were tested and similar results were found.

To understand the reason why the AW approximation is adequate for describing the $2t_r$-t_C-recDIPSHIFT curves of the CH groups, but fails in the case of CH_2 and CH_3, in Figs. 5 and 6 we address the fidelity of the Gaussian approximations (dashed blue lines) for reproducing the general features of the local dipolar field distribution (solid black lines) for CH and CH_2 groups, respectively. The corresponding dipolar spectra were in each case calculated for the (a) rigid and (b) fast motion limits, considering the motion geometries displayed as inset in Fig. 4.

In the rigid limit, both CH and CH_2 dipolar powder patterns, Figs. 5a and 6a, resemble unimodal distributions, so a single second moment can be used in Eq. (4). However, as demonstrated in Figs. 5b and 6b, in the fast-motion limit the pattern for the CH group is still well represented by a single Gaussian, but the pattern for the CH_2 group is clearly composed of two components, i.e., a Pake pattern of about 20 kHz width and an isotropic line. The former arises from the two parallel spin configurations of the two protons, while the latter arises from the antiparallel configurations [48], for which the coupling cancels for the given case of identical dipolar tensors arising from the motional averaging. Thus, the δ-function shaped "central transition" in this spectrum has the same integral intensity as the broad Pake pattern. A similar behavior regarding the bimodal spectrum is also observed for the case of CH_3 groups.

As the core of the AW approximation is that the given frequency distribution can be modeled as a Gaussian, it is straightforward to rationalize the observed behavior, where the description is accurate in describing the $2t_r$-t_C-recDIPSHIFT data of CH groups, but fails for the case of CH_2. This suggests that the scenarios for which the AW approximation is not completely satisfactory (CH_2 and CH_3) may be improved by increasing the number of Gaussian functions used to describe the local field, as demonstrated by the red dotted lines in Fig. 6, which represent a decomposition into two Gaussians.

It is important to remark that the procedure of increasing the number of Gaussians that describe the local field is not straightforward, since in the AW fitting function, Eq. (4), one needs the second-moment pairs M_2^{LT} and M_2^{HT}. As M_2^{HT} depends on the geometry of motion, *a priori* information on the effect of motional

line narrowing of each Gaussian used to describe the local field in the rigid limit is required. Therefore, in the next section we present a geometry-sensitive algebraic method, earlier proposed by Terao and coworkers [48], to decompose the dipolar local field.

4.3. Justification of the double-Gaussian description of CH_n dipolar fields

As already mentioned in the last section, the double-Gaussian approximation for the local dipolar field is justified by earlier work of Terao et al. [48], who proposed the decomposition of a CH_n dipolar powder spectrum into 2^n dipolar powder patterns, each one associated with specific proton spin configurations, see Fig. 7. The principal axes and values of the dipolar tensor corresponding to each component as well as their average values for the fast-motion limit can be obtained on the basis of the spatial arrangement of the CH bonds and the motional geometry, as proposed in Ref. [48].

Fig. 7 exemplifies this decomposition for the case of a CH_2 group executing a planar three-site jump motion. The full dipolar spectrum can be decomposed into 4 components. However, in the rigid limit the dipolar pattern has only two components, since the proton spin configurations $(\uparrow,\uparrow)$, $(\downarrow,\downarrow)$ and $(\uparrow,\downarrow)$, $(\downarrow,\uparrow)$ lead to the same dipolar pattern, see Fig. 7a. Considering a fast three-site jump with the geometry presented in the inset of Fig. 7b, the dipolar patterns associated with the spin configuration $(\uparrow,\downarrow)$, $(\downarrow,\uparrow)$ narrows to an isotropic peak, while the configurations $(\uparrow,\uparrow)$, $(\downarrow,\downarrow)$ correspond to an axially symmetric Pake pattern, see Fig. 7b. Note that the motionally averaged patterns are sensitive to the motional geometry, but can be precisely predicted as described in Ref. [48].

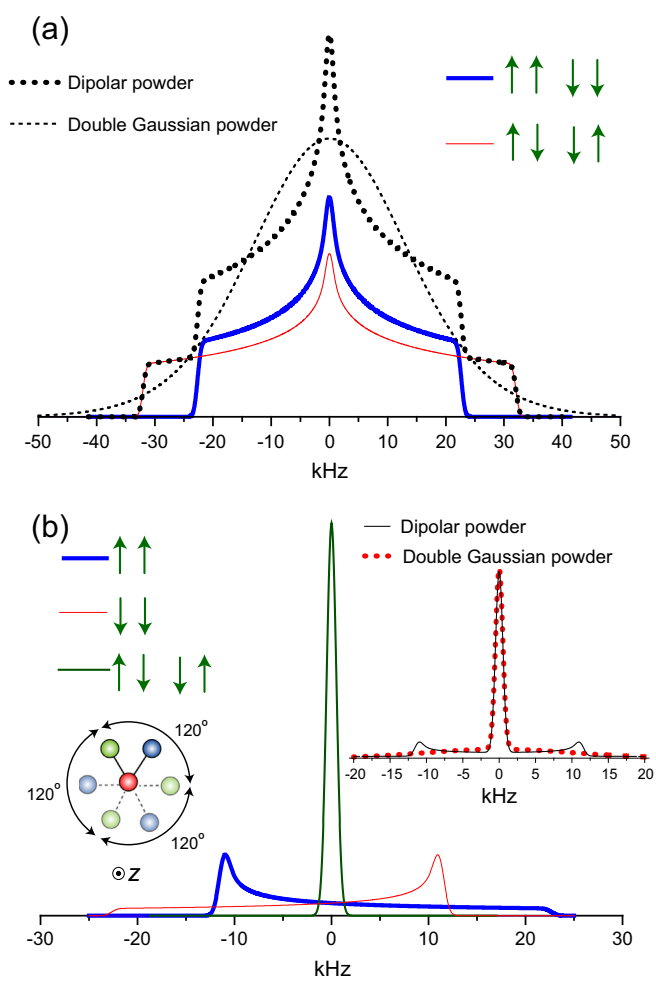

Fig. 7. CH_2 dipolar powder pattern decomposition. (a) Rigid limit, $M_2^{LT}(\uparrow,\uparrow) = M_2^{LT}(\downarrow,\downarrow) = 54.07 \times 10^8\ (\mathrm{rad/s})^2$ and $M_2^{LT}(\uparrow,\downarrow) = M_2^{LT}(\downarrow,\uparrow) = 108.20 \times 10^8\ (\mathrm{rad/s})^2$ and (b) fast limit for the case of a planar three-site jump, with $\beta = 120°$, $M_2^{HT}(\uparrow,\uparrow) = M_2^{HT}(\downarrow,\downarrow) = 40.51 \times 10^8\ (\mathrm{rad/s})^2$ and $M_2^{HT}(\uparrow,\downarrow) = M_2^{HT}(\downarrow,\uparrow) = 0\ (\mathrm{rad/s})^2$. To improve the visualization, the dipolar powder was Gaussian broadened by 500 Hz, but the presented second moments were calculated from the pattern without any broadening, so the Gaussian shape of the central peak in (b) is only due to line broadening.

Given the possibility of decomposing the dipolar local field and calculating the dipolar tensor parameters, one can now approximate each component with a Gaussian local field with the same second moment as the dipolar field components associated with each distinct spin configuration. In general, this gives rise to a multi-Gaussian AW approximation, where the motional effect on each component of the dipolar pattern is considered independently. Nevertheless, one should note that for CH_2 the lower of the two M_2^{HT} is either zero or has a finite value, depending if the motion is evenly uniaxial (3 or more symmetric jump sites) or not. This shows that for CH_2 groups one should never need more than two Gaussians, which stands for a two-Gaussian approximation for the local field, as exemplified by the Gaussian powder in the inset of Fig. 7b. This approach should improve the Gaussian approximation for the local field and consequently render the AW approximation more accurate in describing the $2t_r$-t_C-recDIPSHIFT curves. The details on how to decompose the static and averaged dipolar patterns can be found in Ref. [48]. Since the multi-Gaussian AW approach just relies on the second moments, we only provide the second moments of the decomposed spectrum in each case treated herein.

Fig. 8 shows the spectral decomposition for the case of CH_3 groups. In all cases, the pre-averaging of the dipolar coupling due to fast rotation of the ^1H about the C3 symmetry axis was considered. The rigid limit pattern Fig. 8a can be decomposed into eight spectral components corresponding to the proton spins configurations $(\uparrow,\uparrow,\uparrow)$, $(\uparrow,\uparrow,\downarrow)$, $(\downarrow,\downarrow,\uparrow)$, $(\downarrow,\downarrow,\downarrow)$ plus the permutation of the spin states which independently of the motional regime always renders the same patterns. Thus, despite having 8 spectral components, there are only two different second moments $M_2^{LT} = 39.75 \times 10^8\ (\mathrm{rad/s})^2$ and $M_2^{LT} = 4.43 \times 10^8\ (\mathrm{rad/s})^2$. Considering CH_3 groups executing two-site jumps with reorientation angle of 109°, as in dimethyl sulfone (DMS) molecule, the average tensor is not symmetric, but can be decomposed in only two inequivalent components. For CH_3 groups executing three-site jumps with reorientation angle of 109° (TMSI geometry), the tensors average to eight symmetric components again with only two different second moments. In both geometries, either in the rigid or the fast limit, the ratio between the second moments of the two inequivalent tensor components is 9, which is a consequence of all three tensors being uniaxially pre-averaged and colinear, resulting in a factor 3 in the D values. This shows that also for CH_3 groups only two Gaussian components suffice for the AW treatment. In conclusion, the above discussion shows that for the relevant spin configurations, the maximum number of Gaussian local fields needed for the AW treatment is two, standing for a general two-Gaussian AW approach for describing the effects of motions in SI_n separated local field experiments.

4.4. Double-Gaussian AW approach for $2t_r$-t_C-recDIPSHIFT data

In order to adapt Eq. (4) to a double-Gaussian approximation for the local field, one needs to evaluate the NMR signal for a given local field distribution $P(\omega, t)$ at a given time t. In this case, the NMR signal can be described by the following expression [40]:

$$S(t) = \int_{-\infty}^{\infty} exp(i\omega t)P(\omega, t)\mathrm{d}\omega. \quad (7)$$

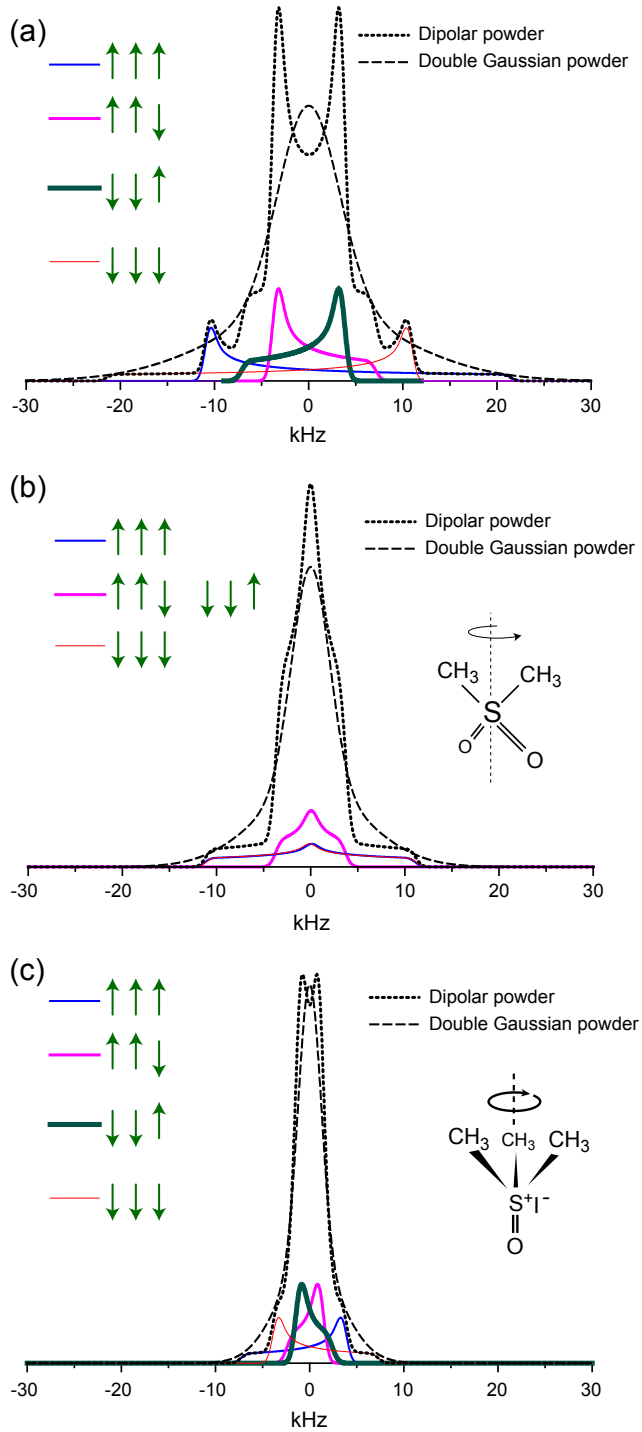

Fig. 8. CH_3 dipolar powder pattern decomposition. (a) Rigid limit, $M_2^{LT}(\uparrow,\uparrow,\uparrow) = M_2^{LT}(\downarrow,\downarrow,\downarrow) = 39.76 \times 10^8\ (\mathrm{rad/s})^2$ and $M_2^{LT}(\uparrow,\uparrow,\downarrow) = M_2^{LT}(\downarrow,\downarrow,\uparrow) = 4.43 \times 10^8\ (\mathrm{rad/s})^2$, (b) fast limit for a CH_3 group executing a two-site jump with the DMS geometry, $M_2^{HT}(\uparrow,\uparrow,\uparrow) = M_2^{HT}(\downarrow,\downarrow,\downarrow) = 13.26 \times 10^8\ (\mathrm{rad/s})^2$ and $M_2^{HT}(\uparrow,\uparrow,\downarrow) = M_2^{HT}(\downarrow,\downarrow,\uparrow) = 1.47 \times 10^8\ (\mathrm{rad/s})^2$, (c) fast limit for a CH_3 group executing a three-site jump with the TMSI geometry, $M_2^{HT}(\uparrow,\uparrow,\uparrow) = M_2^{HT}(\downarrow,\downarrow,\downarrow) = 4.22 \times 10^8\ (\mathrm{rad/s})^2$ and $M_2^{HT}(\uparrow,\uparrow,\downarrow) = M_2^{HT}(\downarrow,\downarrow,\uparrow) = 0.47 \times 10^8\ (\mathrm{rad/s})^2$. To improve the visualization, the dipolar powder was Gaussian broadened by 500 Hz, but the presented second moments was calculated from the pattern without any broadening.

Assuming the local-field distribution to be composed of 2 independent components this becomes:

$$S(t) = \frac{1}{2}\int_{-\infty}^{\infty} exp(i\omega t)\sum_{j=1}^{2} P_j(\omega,t)\mathrm{d}\omega. \tag{8}$$

Therefore, the full signal is simply written as:

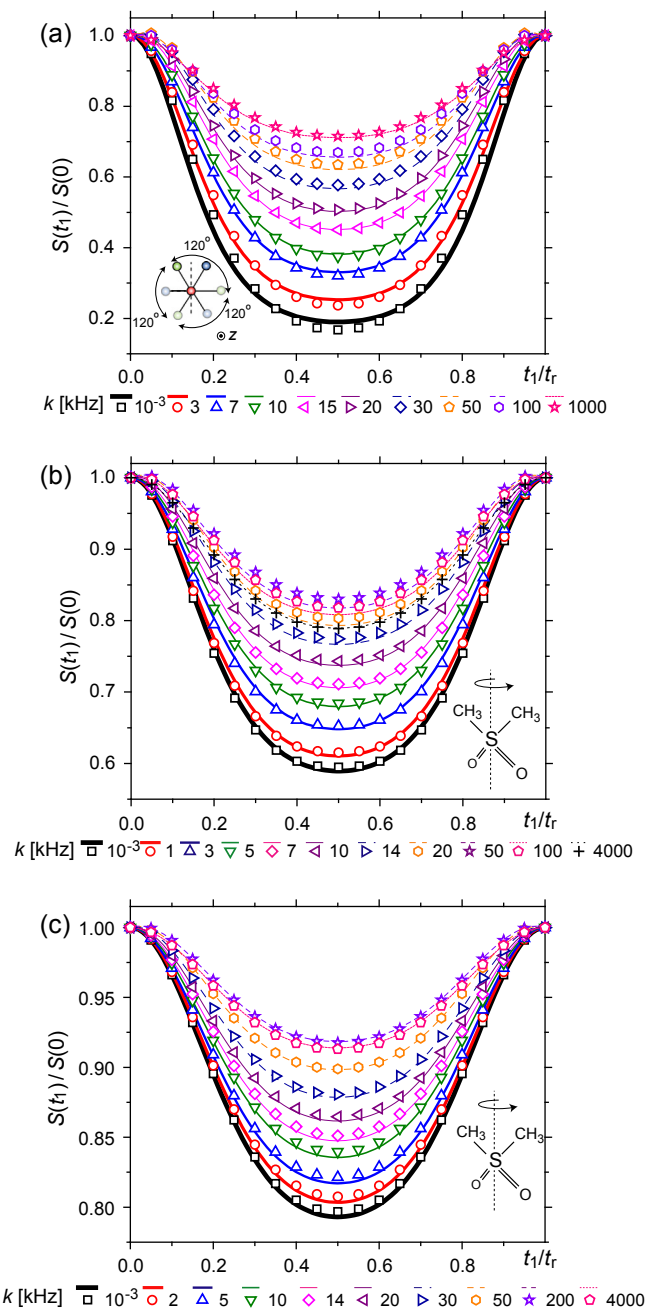

Fig. 9. Comparison between AW approximations using two Gaussians to describe the local field (lines) and dynamic spin dynamics simulations (symbols) for (a, b) $2t_r$-t_C-recDIPSHIFT curves and (c) $4t_r$-t_C-recDIPSHIFT. (a) CH_2 group undergoing a three-site jump with amplitude of motion of 120°, $\nu_r = 16$ kHz, $s^{HT} \times M_2^{LT}(1) = 23.25 \times 10^8\ (\mathrm{rad/s})^2$, $s^{LT} \times M_2^{LT}(2) = 46.53 \times 10^8\ (\mathrm{rad/s})^2$, $s^{HT} \times M_2^{HT}(1) = 15.39 \times 10^8\ (\mathrm{rad/s})^2$ and $s^{HT} \times M_2^{HT}(2) = 0\ (\mathrm{rad/s})^2$. (b) CH_3 group undergoing a two-site jump in the DMS geometry, $\nu_r = 9$ kHz, $s^{LT} \times M_2^{LT}(1) = 71.56 \times 10^7\ (\mathrm{rad/s})^2$, $s^{LT} \times M_2^{LT}(2) = 7.97 \times 10^7\ (\mathrm{rad/s})^2$, $s^{HT} \times M_2^{HT}(1) = 27.85 \times 10^7\ (\mathrm{rad/s})^2$ and $s^{HT} \times M_2^{HT}(2) = 3.09 \times 10^7\ (\mathrm{rad/s})^2$. (c) Same group and geometry as in (b) but $\nu_r = 30$ kHz, $s^{LT} \times M_2^{LT}(1) = 75.53 \times 10^7\ (\mathrm{rad/s})^2$, $s^{LT} \times M_2^{LT}(2) = 8.41 \times 10^7\ (\mathrm{rad/s})^2$, $s^{HT} \times M_2^{HT}(1) = 27.85 \times 10^7\ (\mathrm{rad/s})^2$ and $s^{HT} \times M_2^{HT}(2) = 3.09 \times 10^7\ (\mathrm{rad/s})^2$.

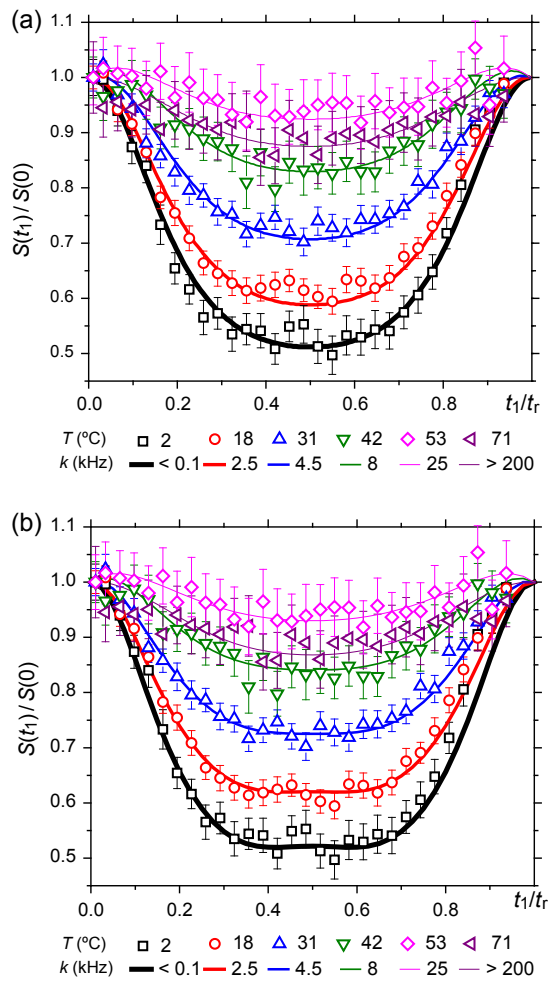

Fig. 10. Best fits for $2t_r$-t_C-recDIPSHIFT modulation curves for TMSI (a) using a two-Gaussian AW approximation with $s^{LT} \times M_2^{LT}(1) = 65.40 \times 10^7$ (rad/s)^2, $s^{LT} \times M_2^{LT}(2) = 7.25 \times 10^7$ (rad/s)^2, $s^{HT} \times M_2^{HT}(1) = 7.18 \times 10^7$ (rad/s)^2 and $s^{HT} \times M_2^{HT}(2) = 0.80 \times 10^7$ (rad/s)^2 and (b) based upon spin dynamics simulations.

$$S(t) = \frac{1}{2}\sum_{j=1}^{2} S_j(t). \tag{9}$$

In practice, Eq. (9) implies that the AW-based fitting function for t_C-recDIPSHIFT considering a two-component local field is the sum of a set of 2 signals $S_j(t)$ obtained according to Eq. (4), with the second moment of each component M_2^{HT} and M_2^{LT} calculated according to the rules of Terao et al. for the decomposition of dipolar fields [48].

Fig. 9 shows a comparison between (a, b)-$2t_r$-t_C-recDIPSHIFT and (c)-$4t_r$-t_C-recDIPSHIFT curves obtained by dynamic spin dynamics simulation (symbols) and by the AW approximation (lines), using two components for the local-field approximation, at several rates of motion: (a) a CH_2 group executing three-site jumps, as illustrated in the inset; (b, c) a CH_3 group undergoing two-site jumps with the DMS geometry, see also the inset of Fig. 9b. As discussed above, in all present cases the dipolar field decomposition embodies two distinct second moments for each motion limit (rigid and fast), and these second moments were used in Eqs. (4) and (9) to obtain an analytical expression for the t_C-recDIPSHIFT curve. Indeed, following the procedure discussed in Section 4.1 to take into account the LG and MAS scaling, the second moments were scaled down by a factor s^i, which was calculated based on the (a, b)-$2t_r$-t_C-recDIPSHIFT and (c)-$4t_r$-t_C-recDIPSHIFT curves in the fast (s^{HT}) and rigid limits (s^{LT}). The scaled second moments are presented in the captions, and follow the calibration shown in Fig. 3b. Contrary to the case of Figs. 4b and c, the perfect agreement between the dynamic spin dynamics simulations and the two-Gaussian AW approach is remarkable even for higher recoupling periods as illustrated in (c) for the $4t_r$-t_C-recDIPSHIFT.

Fig. 10 shows experimental results (symbol) and the best-fit theoretical data (lines) using a) a two-Gaussian AW function and b) dynamic spin dynamics simulation. To fit the experimental result using the two-gaussian AW approximation the scaled second moments in the rigid and fast limit were first determined from the low and high temperature curves. Note that the relative contribution of each Gaussian components is fixed by Teraos theoretical expressions, so the scaling factors s^{HT} and s^{HT} are obtained as a single fit parameter at each limit. These parameters are used to calculate the scaled second moments providing an AW formula, Eq. (4), for each Gaussian component. The AW formulas are summed with equal weight, as in Eq. (9), giving a general fitting function, with the motion rate k as the single fitting parameter. This function is then used to fit the experimental temperature dependence providing the motion rates shown in Fig. 10. Clearly, both methods lead to nearly the same fitted rate of motion for a given temperature which also agree very well with previous results for the same molecule [27].

The given temperatures cover the full dynamic range from the rigid ($T = 2\,°C$, $k = 0.1$ kHz) to the fast limit ($T = 71\,°C$, $k = 200$ kHz), and in analogy to our previous study [33], the $2t_r$-t_C-recDIPSHIFT modulation curves are increasingly shallow, reflecting the apparent averaging of the dipolar tensor. It is important to note that estimations for the high-temperature second moment(s) can only be obtained from fits of the experimental data when one is sufficiently sure that the fast limit is reached, i.e., when the data does not change anymore upon further heating. In this respect, we note in Fig. 10 that the curve at 53° is shallower than that at 71°, which is nicely reproduced in the simulations. Indeed, it is well known that interactions with different strengths gives different T_2 minima as a function o temperature [49]. Based on that, a hypothesis that explain such unusual behavior is that the two components of the local field can lead to different T_2 minima at different temperatures. Despite not seen in our constant-time experiments [33], there is a T_2-related loss of the overall signal, which may changes the relative weighting of the two components at higher temperature producing the observed effect.

Another feature that can be noted in Fig. 10 is that at lower motional rates (at the lowest temperatures) the curves obtained by spin dynamics simulations have a flatter bottom around $t_1 = t_r/2$ than the ones calculated with the AW approach. This highlights the generic limit of the AW approximation already discussed before, when the coupling is too strong and/or the MAS rates is too slow. Even in this situation, by proper scaling of the second moments we find good agreement between the rates calculated using the full treatment and the AW approximation. Note that data at $t_{1,max} = t_r$ corresponds again to short times, as one observes the "back" of the rotor echo, i.e., the AW approximation remains valid at the edges of the modulation interval.

Unfortunately, information about the specific motion geometry is rather limited. This is a general feature of DIPSHIFT experiments because even in an ideal geometry, the amount of the "averaged part" of M_2 varies with the angle, which is a free parameter. So it is difficult to distinguish between a different angle and deviations from the chosen model, which is also to some degree arbitrary. Indeed, one of the advantages of using the AW approach to estimate the motion rates is that it does not depend severely on the motion geometry, but only on the averaged M_2s, making possible to reliably. The detailed evaluation of the motion geometry will

required the use of methods such as Exchange NMR. In this respect, Centerband-Only Detection of Exchange (CODEX) and variants provide an efficient way of separating the effects of the motion geometry and rates [12], but is usually much more time consuming than DIPSHIFT experiments. Also, the motion rates probed by Exchange NMR and DIPSHIFT (or other SLF methods) are in different frequency scales, so they are indeed complementary [13].

5. Conclusions

Based upon recent work of Hirschinger [32], a combination of the Anderson–Weiss and memory-function approximations was used to derive a fitting formula that describes NMR signals obtained in t_C-recDIPSHIFT SLF experiments. By comparing motion-dependent t_C-recDIPSHIFT modulation curves obtained from the derived formula and results from dynamic spin dynamics simulations, we concluded that for SI spin pairs the usual single-Gaussian AW approach is rather accurate in describing the full t_C-recDIPSHIFT modulation curves. However, considering more (n) abundant (^{1}H) I spins coupled to the observed S spin (I_n–S spin system), the analytical approximation failed in describing the data in the intermediate and fast limits. The origin of this limitation in the dynamic range of was found to be related to the poor accuracy of the single-Gaussian approximation in describing the I_n–S local field, in particular when molecular motions are considered and inhomogeneous spectral narrowing takes place.

Therefore, an AW treatment based upon a double-Gaussian approximation for the dipolar local field was proposed. Using this approach, an analytical formula for the t_C-recDIPSHIFT signal was derived, adapted to take into account a double-Gaussian local field, which was evidenced to be very accurate in describing the molecular-motion effect on the modulation curves in I_n–S spin systems. Specifically, $2t_r$-t_C-recDIPSHIFT experiments were performed as function of the temperature in a model sample, and, using the derived fitting function considering a two-component local field, the rates of motion obtained as function of the temperature coincided perfectly with those obtained on the basis of full dynamical spin dynamics simulations. We expect the new AW-approach to be of general use in studying the dynamics of I_n–S moieties in synthetic and possibly biomolecular materials and molecules.

Acknowledgments

This project was executed in the framework of the projects 2009/18354-8 and 2008/11675-0 funded by the Brazilian funding agency FAPESP and the CAPES/DAAD PROBRAL exchange project (proc. 330/09 – Brasilian side and D/08/11622 and 50752585 – German side), as well as of the FOR 1145 project SA 982/7-2 funded by the Deutsche Forschungsgemeinschaft (DFG).

References

[1] G.C. Faria, R.M. Faria, E.R. deAzevedo, H. von Seggern, Temperature dependence of the drift mobility of poly(9,9′-dioctylfluorene-co-benzothiadiazole)-based thin-film devices, J. Phys. Chem. C 115 (51) (2011) 25479–25483.
[2] G.C. Faria, T.S. Plivelic, R.F. Cossiello, A.A. Souza, T.D.Z. Atvars, I.L. Torriani, E.R. deAzevedo, A multitechnique study of structure and dynamics of polyfluorene cast films and the influence on their photoluminescence, J. Phys. Chem. B 113 (33) (2009) 11403–11413.
[3] M. Hofmann, A. Herrmann, S. Ok, C. Franz, D. Kruk, K. Saalwächter, M. Steinhart, E.A. Rössler, Polymer dynamics of polybutadiene in nanoscopic confinement as revealed by field cycling ^{1}H NMR, Macromolecules 44 (11) (2011) 4017–4021.
[4] F. Hu, W. Luo, M. Hong, Mechanisms of proton conduction and fating in influenza M2 proton channels from solid-state NMR, Science 330 (6003) (2010) 505–508.
[5] J.L. Valentin, P. Posadas, A. Fernandez-Torres, M.A. Malmierca, L. Gonzalez, W. Chasse, K. Saalwächter, Inhomogeneities and chain dynamics in diene rubbers vulcanized with different cure systems, Macromolecules 43 (9) (2010) 4210–4222.
[6] S. Faske, H. Eckert, M. Vogel, ^{6}Li and ^{7}Li NMR line-shape and stimulated-echo studies of lithium ionic hopping in $LiPO_3$ glass, Phys. Rev. B 77 (10) (2008) 104301.
[7] O.S. Andersen, R.E. Koeppe II, Bilayer thickness and membrane protein function: an energetic perspective, Annu. Rev. Biophys. Biomol. Struct. 36 (2007) 107–130.
[8] S. Brown, H. Spiess, Advanced solid-state NMR methods for the elucidation of structure and dynamics of molecular, macromolecular, and supramolecular systems, Chem. Rev. 101 (12) (2001) 4125–4155.
[9] A.G. Palmer, C.D. Kroenke, J.P. Loria, Nuclear magnetic resonance methods for quantifying microsecond-to-millisecond motions in biological macromolecules, Methods Enzym. 339 (2001) 204–238.
[10] J.H. Davis, The description of membrane lipid conformation, order and dynamics by ^{2}H-NMR, Biochim. Biophys. Acta 737 (1983) 117–171.
[11] E.R. deAzevedo, S.B. Kennedy, M. Hong, Determination of slow motions in extensively isotopically labeled proteins by magic-angle-spinning ^{13}C-detected ^{15}N-exchange NMR, Chem. Phys. Lett. 321 (1–2) (2000) 43–48.
[12] D. Reichert, O. Pascui, T. Bonagamba, E. deAzevedo, A. Schmidt, Scaling-down the CSA recoupling in S-CODEX 1D-MAS exchange experiments, Chem. Phys. Lett. 380 (5–6) (2003) 583–588.
[13] A. Krushelnitsky, D. Reichert, K. Saalwchter, Solid-state NMR approaches to internal dynamics of proteins: from picoseconds to microseconds and seconds, Acc. Chem. Res. 46 (2013) 2444–2453.
[14] J. Yang, L. Aslimovska, C. Glaubitz, Molecular dynamics of proteorhodopsin in lipid bilayers by solid-state NMR, J. Am. Chem. Soc. 133 (13) (2011) 4874–4881.
[15] A. Krushelnitsky, T. Zinkevich, N. Mukhametshina, N. Tarasova, Y. Gogolev, O. Gnezdilov, V. Fedotov, P. Belton, D. Reichert, C-13 and N-15 NMR study of the hydration response of T4 lysozyme and alpha B-crystallin internal dynamics, J. Phys. Chem. B 113 (29) (2009) 10022–10034.
[16] P. Zhu, J. Xu, N. Sahar, M.D. Morris, D.H. Kohn, A. Ramamoorthy, Time-resolved dehydration-induced structural changes in an intact bovine cortical bone revealed by solid-state NMR spectroscopy, J. Am. Chem. Soc. 131 (47) (2009) 17064–17065.
[17] W. Chen, H. Sun, T. Miyoshi, Unique molecular dynamics of structural elements in an asymmetric janus bisamide supramolecule characterized by solid-state NMR, J. Phys. Chem. B 117 (2013) 13698–13709.
[18] K. Schaler, A. Achilles, R. Barenwald, C. Hackel, K. Saalwächter, Dynamics in crystallites of poly(epsilon-caprolactone) as investigated by solid-state NMR, Macromolecules 46 (2013) 7818–7825.
[19] T. Bonagamba, F. Becker-Guedes, E. deAzevedo, K. Schimidt-Rohr, Slow ester side-group flips in glassy poly(alkyl methacrylate)s characterized by centerband-only detection of exchange nuclear magnetic resonance, J. Polym. Sci., Part B: Polym. Phys. 39 (2001) 2028–2036.
[20] D. Reichert, NMR studies of dynamic processes in organic solids, Annu. Rep. NMR Spectrosc. 55 (2005) 159–203.
[21] M. Munowitz, R.G. Griffin, G. Bodenhausen, T.H. Huang, Two-dimensional rotational spin-echo nuclear magnetic resonance in solids: correlation of chemical shift and dipolar interaction, J. Am. Chem. Soc. 103 (1981) 2529–2533.
[22] A. Ramamoorthy, S. Opella, Two-dimensional chemical shift/hetero-nuclear dipolar coupling spectra obtained with polarization inversion spin exchange at the magic angle and magic-angle sample spinning (PISEMA-MAS), Solid State Nucl. Magn. Reson. 4 (1995) 387–392.
[23] K. Yamamoto, V. Ermakov, D. Lee, A. Ramamoorthy, PITANSEMA-MAS, a solid-state NMR method to measure hetero-nuclear dipolar couplings under MAS, Chem. Phys. Lett. 408 (2005) 118–122.
[24] D. Reichert, O. Pascui, E.R. deAzevedo, T.J. Bonagamba, K. Arnold, D. Huster, A solid-state nmr study of the fast and slow dynamics of collagen fibrils at varying hydration levels, Magn. Reson. Chem. 42 (2) (2004) 276–284.
[25] J. Lorieau, A. Mc Dermott, Order parameters based on ^{13}C^{1}H, ^{13}C^{1}H$_2$ and ^{13}C^{1}H^3 hetero-nuclear dipolar powder patterns: a comparison of MAS-based solid-state NMR sequences, Magn. Reson. Chem. 148 (2006) 334–347.
[26] S. Theisgen, H.A. Scheidt, A. Magalhaes, T.J. Bonagamba, D. Huster, A solid-state NMR study of the structure and dynamics of the myristoylated N-terminus of the guanylate cyclase-activating protein-2, Biochim. Biophys. Acta 1798 (2010) 266–274.
[27] E.R. deAzevedo, K. Saalwächter, O. de Pascui, A.A. Souza, T.J. Bonagamba, D. Reichert, Intermediate motions as studied by solid-state separated local field NMR experiments, J. Chem. Phys 128 (10) (2008) 104505.
[28] M.F. Cobo, K. Malinakova, D. Reichert, K. Saalwächter, E.R. deAzevedo, Intermediate motions and dipolar couplings as studied by Lee–Goldburg cross-polarization NMR: Hartmann–Hahn matching profiles, Phys. Chem. Chem. Phys. 11 (32) (2009) 7036–7047.
[29] K. Saalwächter, I. Fischbach, The application of MAS recoupling methods in the intermediate motional regime, J. Magn. Reson. 157 (1) (2002) 17–30.
[30] M. Veshtort, R.G. Griffin, SPINEVOLUTION: a powerful tool for the simulation of solid and liquid state NMR experiments, J. Magn. Reson. 178 (2) (2006) 248–282.
[31] P.W. Anderson, P.R. Weiss, Exchange narrowing in paramagnetic resonance, Rev. Mod. Phys. 25 (1) (1953) 269–276.
[32] J. Hirschinger, Analytical solutions to several magic-angle spinning NMR experiments, Solid. Stat. Nucl. Magn. Reson. 34 (4) (2008) 210–223.
[33] M.F. Cobo, A. Achilles, D. Reichert, E.R. deAzevedo, K. Saalwächter, Recoupled separated-local-field experiments and applications to study intermediate-regime molecular motions, J. Magn. Reson. 221 (2012) 85–96.

[34] M. Hong, J.D. Gross, C.M. Rienstra, R.G. Griffin, K.K. Kumashiro, K. Schmidt-Rohr, Coupling amplification in 2D MAS NMR and its application to torsion angle determination in peptides, J. Magn. Reson. 129 (1) (1997) 85–92.
[35] T. Gullion, J. Schaefer, Rotational-echo double-resonance NMR, J. Magn. Reson. 81 (1) (1989) 196–200.
[36] M. Lee, W.I. Goldburg, Nuclear magnetic resonance line narrowing by a rotating RF field, Phys. Rev. 140 (4A) (1965) 1261–1268.
[37] E. Vinogradov, P.K. Madhu, S. Vega, Phase modulated Lee–Goldburg magic angle spinning proton nuclear magnetic resonance experiments in the solid state: a bimodal Floquet theoretical treatment, J. Chem. Phys. 115 (19) (2001) 8983–9000.
[38] A. Abragam, Principles of Nuclear Magnetism, Oxford University Press, Oxford, 1983.
[39] F. Engelke, T. Kind, D. Michel, M. Pruski, B.C. Gerstein, A theoretical approach for the calculation of the Hartmann–Hahn matching under cross polarization and magic-angle spinning, J. Magn. Reson. 95 (1991) 286–298.
[40] J. Hirschinger, A simple analytical model to describe dynamic magic-angle spinning experiments, Conc. Magn. Reson. Part A 28A (5) (2006) 307–320.
[41] F.V. Chavez, K. Saalwaechter, Time-domain NMR observation of entangled polymer dynamics: analytical theory of signal functions, Macromolecules 44 (6) (2011) 1560–1569.
[42] N. Fatkullin, A. Gubaidullin, C. Mattea, S. Stapf, On the theory of the proton free induction decay and Hahn echo in polymer systems: the role of intermolecular magnetic dipole–dipole interactions and the modified Anderson–Weiss approximation, J. Chem. Phys. 137 (2012) 224907.
[43] J. Vanvleck, The dipolar broadening of magnetic resonance lines in crystals, Phys. Rev. 74 (9) (1974) 1168–1183.
[44] M. Bertmer, H. Eckert, Dephasing of spin echoes by multiple heteronuclear dipolar interactions in rotational echo double resonance NMR experiments, Solid. Stat. Nucl. Magn. Reson. 15 (3) (1999) 139–152.
[45] K. Saalwächter, R. Graf, H. Spiess, Recoupled polarization-transfer methods for solid-state $^{1}H^{13}C$ hetero-nuclear correlation in the limit of fast MAS, J. Magn. Reson. 148 (2001) 398–418.
[46] J. Demers, V. Chevelkov, A. Lange, Progress in correlation spectroscopy at ultra-fast magic-angle spinning: basic building blocks and complex experiments for the study of protein structure and dynamics, Solid. Stat. Nucl. Magn. Reson. 40 (3) (2011) 101–113.
[47] P. Palucha, T. Pawlak, J. Amoureux, M. Potrzebowsk, Simple and accurate determination of XH distances under ultra-fast MAS NMR, J. Magn. Reson. 233 (2013) 56–63.
[48] T. Terao, H. Miura, A. Saika, Dipolar SASS NMR-spectroscopy – separation of heteronuclear dipolar powder patterns in rotating solids, J. Chem. Phys. 85 (7) (1986) 3816–3826.
[49] D. Reichert, G. Hempel, H. Zimmermann, H. Schneider, Z. Luz, Dynamic carbon-13 MAS NMR: application to benzene ring flips in polyaryl ethers, Solid State Nucl. Magn. Reson. 18 (2000) 17–36.